Inorganic Chemistry

pubs.acs.org/IC Article

Structural Diversity in Molecular Nickel Phosphide Carbonyl Nanoclusters

Chiara Capacci, Cristiana Cesari, Cristina Femoni, Maria Carmela Iapalucci, Federica Mancini, Silvia Ruggieri, and Stefano Zacchini*

Cite This: *Inorg. Chem.* 2020, 59, 16016−16026 Read Online

ACCESS | Metrics & More | Article Recommendations | Supporting Information

ABSTRACT: The reaction of $[Ni_6(CO)_{12}]^{2-}$ as a $[NBu_4]^+$ salt in CH_2Cl_2 with 0.8 equiv of PCl_3 afforded $[Ni_{14}P_2(CO)_{22}]^{2-}$. In contrast, the reactions of $[Ni_6(CO)_{12}]^{2-}$ as a $[NEt_4]^+$ salt with 0.4−0.5 equiv of $POCl_3$ afforded $[Ni_{22-x}P_2(CO)_{29-x}]^{4-}$ (x = 0.84) or $[Ni_{39}P_3(CO)_{44}]^{6-}$ by using CH_3CN and thf as a solvent, respectively. Moreover, by using 0.7−0.9 mol of $POCl_3$ per mole of $[NEt_4]_2[Ni_6(CO)_{12}]$ both in CH_3CN and thf, $[Ni_{23-x}P_2(CO)_{30-x}]^{4-}$ (x = 0.82) was obtained together with $[Ni_{22}P_6(CO)_{30}]^{2-}$ as a side product. $[Ni_{23-x}P_2(CO)_{30-x}]^{4-}$ (x = 0.82) and $[Ni_{22}P_6(CO)_{30}]^{2-}$ were separated owing to their different solubility in organic solvents. All the new molecular nickel phosphide carbonyl nanoclusters were structurally characterized through single crystal X-ray diffraction (SC-XRD) as $[NBu_4]_2[Ni_{14}P_2(CO)_{22}]$ (two different polymorphs, $P2_1/n$ and $C2/c$), $[NEt_4]_4[Ni_{23-x}P_2(CO)_{30-x}]\cdot CH_3COCH_3\cdot$solv ($x$ = 0.82), $[NEt_4]_2[Ni_{22}P_6(CO)_{30}]\cdot$2thf, $[NEt_4]_4[Ni_{22-x}P_2(CO)_{29-x}]\cdot 2CH_3COCH_3$(x = 0.84) and $[NEt_4]_6[Ni_{39}P_3(CO)_{44}]\cdot C_6H_{14}\cdot$solv. The metal cores' sizes of these clusters range from 0.59 to 1.10 nm, and their overall dimensions including the CO ligands are 1.16−1.63 nm. In this respect, they are comparable to ultrasmall metal nanoparticles, molecular nanoclusters, or atomically precise metal nanoparticles. The environment of the P atoms within these molecular Ni−P−CO nanoclusters displays a rich diversity, that is, Ni_5P pentagonal pyramid, Ni_7P monocapped trigonal prism, Ni_8P bicapped trigonal prism, Ni_9P monocapped square antiprism, $Ni_{10}P$ sphenocorona, $Ni_{10}P$ bicapped square antiprism, and $Ni_{12}P$ icosahedron.

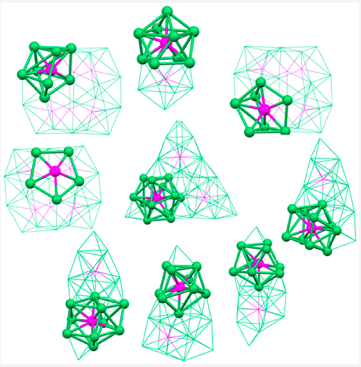

INTRODUCTION

The Ni−P phase diagram is very rich, and 11 different phases have been identified, that is, Ni_3P, Ni_8P_3, $Ni_{12}P_5$, Ni_2P, Ni_5P_4, NiP (one monoclinic and two orthorhombic structures), NiP_2 (cubic and monoclinic), and NiP_3.[1−5] Ni-rich phases (Ni_3P, Ni_8P_3, $Ni_{12}P_5$, Ni_2P) show isolated P atoms inside tricapped trigonal prismatic, monocapped square antiprismatic, cubic, or sphenocorona Ni cages. Conversely, direct P−P bonds are present in P-richer phases, affording P_2, P_3, and P_4 units or longer chains.

Nickel phosphides, particularly as nanoparticles, are very interesting for applications in catalysis and electrocatalysis, in particular as alternatives to noble-metal catalysts.[6−13] Ni_2P supported on silica displays good activity in hydrodesulfurization (HDS) and hydrodenitrization (HDN).[14,15] $Ni_{12}P_5$ nanoparticles have been demonstrated to be good catalysts in electrolytic and photoelectrolytic processes for hydrogen generation.[16,17] Generally speaking, nickel phosphides are viewed as promising noble-metal-free catalysts for water splitting.[18−21]

Only two molecular Ni−P carbonyl nanoclusters have been characterized so far, that is, $[Ni_{11}P(CO)_{18}]^{3-}$ and $[H_{6-n}Ni_{31}P_4(CO)_{39}]^{n-}$ (n = 4, 5).[22] The unique P atom of $[Ni_{11}P(CO)_{18}]^{3-}$ is enclosed within a Ni_{10} spheonocorona cage, whereas $[H_{6-n}Ni_{31}P_4(CO)_{39}]^{n-}$ (n = 4, 5) contains two distorted Ni_9P monocapped square antiprisms and two distorted $Ni_{10}P$ bicapped square antiprisms. $[H_{6-n}Ni_{31}P_4(CO)_{39}]^{n-}$ (n = 4, 5) also represents the largest structurally characterized metal carbonyl cluster containing P atoms. Indeed, several Co, Rh, Ru, and Os phosphide carbonyl clusters are known, but with a nuclearity of 6−10 and containing 1−2 P atoms.[23−30] Due to the larger radius of Os compared to Rh and Ru, phosphorus is enclosed within a trigonal prismatic cage in the case of Os clusters, whereas it requires larger square antiprismatic cages for Rh and Ru. Because of the even smaller size of cobalt, P atoms may be both fully interstitial (within capped square antiprismatic cages) and semi-interstitial.

Aiming at widening the scope of our work, we have attempted synthesis and structural characterization by single-crystal X-ray diffraction (SC-XRD) of other nickel phosphide carbonyl nanoclusters. Herein, we present the new fully interstitial polyphosphides $[Ni_{14}P_2(CO)_{22}]^{2-}$,

Received: August 28, 2020
Published: October 21, 2020

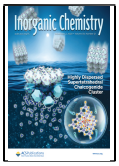

https://dx.doi.org/10.1021/acs.inorgchem.0c02572
Inorg. Chem. 2020, 59, 16016−16026

Scheme 1. Synthesis of Ni−P−CO Clusters

$$[NEt_4]_2[Ni_6(CO)_{12}] \xrightarrow[\text{in thf}]{+0.5\ PCl_3} [Ni_{11}P(CO)_{18}]^{3-} \xrightarrow[\text{in thf}]{+0.3\ PCl_3} [HNi_{31}P_4(CO)_{39}]^{5-} \quad (1)$$

$$[NBu_4]_2[Ni_6(CO)_{12}] \xrightarrow[\text{in } CH_2Cl_2]{+0.8\ PCl_3} [Ni_{14}P_2(CO)_{22}]^{2-} \quad (2)$$

$$[NEt_4]_2[Ni_6(CO)_{12}] \xrightarrow[\text{in } CH_3CN]{+0.4\text{-}0.5\ POCl_3} [Ni_{22-x}P_2(CO)_{29-x}]^{4-}\ (x = 0.84) \quad (3)$$

$$[NEt_4]_2[Ni_6(CO)_{12}] \xrightarrow[\text{in thf}]{+0.4\text{-}0.5\ POCl_3} [Ni_{39}P_3(CO)_{44}]^{6-} \quad (4)$$

$$[NEt_4]_2[Ni_6(CO)_{12}] \xrightarrow[\text{in thf or } CH_3CN]{+0.7\text{-}0.9\ POCl_3} [Ni_{23-x}P_2(CO)_{30-x}]^{4-}\ (x = 0.82)^* \quad (5)$$

* $[Ni_{22}P_6(CO)_{30}]^{2-}$ is obtained as side-product

$[Ni_{23-x}P_2(CO)_{30-x}]^{4-}$ (x = 0.82), $[Ni_{22-x}P_2(CO)_{29-x}]^{4-}$ (x = 0.84), and $[Ni_{39}P_3(CO)_{44}]^{6-}$, as well as the $[Ni_{22}P_6(CO)_{30}]^{2-}$ cluster, which contains fully interstitial, semi-interstitial, and exposed P atoms. The structural diversity of these Ni−P nanoclusters is discussed.

EXPERIMENTAL SECTION

General Procedures. All reactions and sample manipulations were carried out using standard Schlenk techniques under nitrogen and in dried solvents. All of the reagents were commercial products (Aldrich) of the highest purity available and used as received, except $[NR_4]_2[Ni_6(CO)_{12}]$ (R = Et, Bu), which has been prepared according to the literature.[31] Analysis of Ni was performed by atomic absorption on a Pye-Unicam instrument. Analyses of C, H, and N were obtained with a Thermo Quest Flash EA 1112NC instrument. IR spectra were recorded on a PerkinElmer Spectrum One interferometer in CaF_2 cells. $^{31}P\{^1H\}$ NMR measurements were performed on a Varian Mercury Plus 400 MHz instrument. The phosphorus chemical shifts were referenced to external H_3PO_4 (85% in D_2O). Structure drawings have been performed with SCHAKAL99[32] and Mercury 2020.1.[33]

Warning! *CO and $Ni(CO)_4$ may be generated during manipulation of these compounds. All of the operations must be carried out under a well-ventilated fume hood.*

Synthesis of $[NBu_4]_2[Ni_{14}P_2(CO)_{22}]$. A solution of PCl_3 (0.182 g, 1.33 mmol) in CH_2Cl_2 (30 mL) was added to a solution of $[NBu_4]_2[Ni_6(CO)_{12}]$ (1.65 g, 1.49 mmol) in CH_2Cl_2 (20 mL) over a period of 4 h. The resulting mixture was stirred at room temperature for 1 h and, then, the solvent removed *in vacuo*. The residue was washed with H_2O (3 × 20 mL) and extracted with CH_2Cl_2 (20 mL). Crystals of $[NBu_4]_2[Ni_{14}P_2(CO)_{22}]$ suitable for X-ray analyses were obtained by layering *n*-hexane (40 mL) on the CH_2Cl solution (yield 0.70 g, 55% based on Ni). Two different polymorphs, space groups $P2_1/n$ and $C2/c$, were obtained.

$C_{54}H_{72}N_2Ni_{14}O_{22}P_2$ (1985.02), calcd.: C 32.84, H 3.68, N 1.42. Found: C 32.57, H 3.89, N 1.19. IR (CH_2Cl_2, 293 K), ν_{CO}: 2032(s), 1862(m) cm^{-1}. IR (CH_3CN, 293 K), ν_{CO}: 2026(s), 1863(m) cm^{-1}.

Synthesis of $[NEt_4]_4[Ni_{23-x}P_2(CO)_{30-x}]\cdot CH_3COCH_3$·solv ($x$ = 0.82). A solution of $POCl_3$ (0.310 g, 2.02 mmol) in CH_3CN (15 mL) was added to a solution of $[NEt_4]_2[Ni_6(CO)_{12}]$ (2.39 g, 2.52 mmol) in CH_3CN (50 mL) over a period of 4 h. The resulting mixture was stirred at room temperature for 1 h and, then, the solvent removed *in vacuo*. The residue was washed with H_2O (3 × 20 mL), thf (3 × 20 mL), and extracted with CH_3COCH_3 (20 mL). Crystals of $[NEt_4]_4[Ni_{23-x}P_2(CO)_{30-x}]\cdot CH_3COCH_3$·solv ($x$ = 0.82) suitable for X-ray analyses were obtained by layering *n*-hexane (40 mL) on the acetone solution (yield 0.73 g, 39% based on Ni).

$C_{64.18}H_{86}N_4Ni_{22.18}O_{30.18}P_2$ (2760.97), calcd.: C 28.08, H 3.16, N 2.04. Found: C 27.85, H 3.33, N 1.84. IR (CH_3CN, 293 K) ν_{CO}: 2004(s), 1865(ms) cm^{-1}.

Synthesis of $[NEt_4]_2[Ni_{22}P_6(CO)_{30}]\cdot 2thf$. A solution of $POCl_3$ (0.284 g, 1.85 mmol) in thf (15 mL) was added to a solution of $[NEt_4]_2[Ni_6(CO)_{12}]$ (2.42 g, 2.55 mmol) in thf (50 mL) over a period of 4 h. The resulting mixture was stirred at room temperature for 1 h and, then, the solvent removed *in vacuo*. The residue was washed with H_2O (3 × 20 mL) and extracted with thf (20 mL). [The residue not soluble in thf was further extracted with acetone (20 mL). The IR spectrum of the acetone solution is identical to that of $[NEt_4]_4[Ni_{23-x}P_2(CO)_{30-x}]\cdot 2CH_3COCH_3$.] Crystals of $[NEt_4]_2[Ni_{22}P_6(CO)_{30}]\cdot 2thf$ suitable for X-ray analyses were obtained by layering *n*-hexane (40 mL) on the thf solution (yield 0.15 g, 8% based on Ni).

$C_{54}H_{56}N_2Ni_{22}O_{32}P_6$ (2722.44), calcd.: C 23.96, H 2.09, N 1.04. Found: C 23.79, H 2.21, N 0.88. IR (nujol, 293 K), ν_{CO}: 2032(vs), 1991(ms), 1931(m), 1844(m), 1825(m) cm^{-1}. IR (thf, 293 K), ν_{CO}: 2031(vs), 1943(w), 1836(m) cm^{-1}.

Synthesis of $[NEt_4]_4[Ni_{22-x}P_2(CO)_{29-x}]\cdot 2CH_3COCH_3$ (x = 0.84). A solution of $POCl_3$ (0.144 g, 0.941 mmol) in CH_3CN (5 mL) was added to a solution of $[NEt_4]_2[Ni_6(CO)_{12}]$ (2.16 g, 2.28 mmol) in CH_3CN (50 mL) over a period of 4 h. The resulting mixture was stirred at room temperature for 1 h and, then, the solvent removed *in vacuo*. The residue was washed with H_2O (3 × 20 mL), thf (3 × 20 mL), and extracted with CH_3COCH_3 (20 mL). Crystals of $[NEt_4]_4[Ni_{22-x}P_2(CO)_{29-x}]\cdot 2CH_3COCH_3$ (x = 0.84) suitable for X-ray analyses were obtained by layering *n*-hexane (40 mL) on the acetone solution (yield 0.63 g, 36% based on Ni).

$C_{66.16}H_{92}N_4Ni_{21.16}O_{30.16}P_2$ (2730.37), calcd.: C 29.26, H 3.42, N 2.06. Found: C 29.04, H 3.61, N 1.79. IR (nujol, 293 K), ν_{CO}: 2026(sh), 1993(vs), 1966(m), 1948(sh), 1834(s) cm^{-1}. IR (acetone, 293 K), ν_{CO}: 1997(vs), 1963(sh), 1870(s) cm^{-1}. IR (CH_3CN, 293 K), ν_{CO}: 2003(vs), 1962(sh), 1869(s) cm^{-1}. IR (dmso, 293 K), ν_{CO}: 1993(vs), 1960(sh), 1863(s) cm^{-1}.

Synthesis of $[NEt_4]_6[Ni_{39}P_3(CO)_{44}]\cdot C_6H_{14}$·solv. A solution of $POCl_3$ (0.193 g, 1.26 mmol) in thf (20 mL) was added to a solution of $[NEt_4]_2[Ni_6(CO)_{12}]$ (2.39 g, 2.52 mmol) in thf (50 mL) over a period of 4 h. The resulting mixture was stirred at room temperature for 1 h and, then, the solvent removed *in vacuo*. The residue was washed with H_2O (3 × 20 mL), thf (3 × 20 mL), and CH_3COCH_3 (3 × 20 mL) and extracted with CH_3CN (20 mL). Crystals of $[NEt_4]_6[Ni_{39}P_3(CO)_{44}]\cdot C_6H_{14}$·solv suitable for X-ray analyses were obtained by layering *n*-hexane (2 mL) and di-iso-propyl-ether (40 mL) on the CH_3CN solution (yield 0.18 g, 10% based on Ni).

$C_{98}H_{134}N_6Ni_{39}O_{44}P_3$ (4482.70), calcd.: C 26.42, H 3.03, N 1.89. Found: C 26.61, H 3.22, N 1.68, Ni 46.04. IR (CH_3CN, 293 K), ν_{CO}: 1998(vs), 1868(s) cm^{-1}.

X-ray Crystallographic Study. Crystal data and collection details for $[NBu_4]_2[Ni_{14}P_2(CO)_{22}]$ ($P2_1/n$), $[NBu_4]_2[Ni_{14}P_2(CO)_{22}]$ ($C2/c$), $[NEt_4]_4[Ni_{23-x}P_2(CO)_{30-x}]\cdot CH_3COCH_3$·solv ($x$ = 0.82), $[NEt_4]_2[Ni_{22}P_6(CO)_{30}]\cdot 2thf$, $[NEt_4]_4[Ni_{22-x}P_2(CO)_{29-x}]\cdot 2CH_3COCH_3$ (x = 0.84), and $[NEt_4]_6[Ni_{39}P_3(CO)_{44}]\cdot C_6H_{14}$·solv

https://dx.doi.org/10.1021/acs.inorgchem.0c02572
Inorg. Chem. 2020, 59, 16016−16026

are reported in Table S1 in the Supporting Information. ORTEP drawings of all the structures are included in Figures S5−S9 in the Supporting Information. The diffraction experiments were carried out on a Bruker APEX II diffractometer equipped with a CCD detector ($[NBu_4]_2[Ni_{14}P_2(CO)_{22}]$ ($P2_1/n$), $[NBu_4]_2[Ni_{14}P_2(CO)_{22}]$ ($C2/c$), $[NEt_4]_4[Ni_{23-x}P_2(CO)_{30-x}]\cdot CH_3COCH_3\cdot$solv ($x$ = 0.82), $[NEt_4]_6[Ni_{39}P_3(CO)_{44}]\cdot C_6H_{14}\cdot$solv), or a PHOTON2 detector ($[NEt_4]_4[Ni_{22-x}P_2(CO)_{29-x}]\cdot 2CH_3COCH_3$ (x = 0.84) and $[NEt_4]_2[Ni_{22}P_6(CO)_{30}]\cdot$2thf) using Mo K$\alpha$ radiation. Data were corrected for Lorentz polarization and absorption effects (empirical absorption correction SADABS).[34] Structures were solved by direct methods and refined by full-matrix least-squares based on all data using F^2.[35] Hydrogen atoms were fixed at calculated positions and refined by a riding model. All non-hydrogen atoms were refined with anisotropic displacement parameters, unless otherwise stated. Further details are given in the Supporting Information.

RESULTS AND DISCUSSION

The synthesis of Ni−P−CO clusters is very sensitive to experimental conditions (Scheme 1), that is, the stoichiometric ratio, counterion, solvent, and P source. Thus, by reacting $[Ni_6(CO)_{12}]^{2-}$ as a $[NEt_4]^+$ salt with PCl_3 in thf, $[Ni_{11}P(CO)_{18}]^{3-}$ and, then, $[HNi_{31}P_4(CO)_{39}]^{5-}$ were formed in sequence, as previously reported.[22] Conversely, carrying out a similar reaction in CH_2Cl_2 with $[NBu_4]^+$ as a counterion, $[Ni_{14}P_2(CO)_{22}]^{2-}$ was obtained. When $POCl_3$ was used instead of PCl_3, the products observed were $[Ni_{22-x}P_2(CO)_{29-x}]^{4-}$ (x = 0.84) by using 0.4−0.5 mol of $POCl_3$ per mole of $[NEt_4]_2[Ni_6(CO)_{12}]^{2-}$ in CH_3CN or $[Ni_{39}P_3(CO)_{44}]^{6-}$ by performing the same reaction in thf. In contrast, $[Ni_{23-x}P_2(CO)_{30-x}]^{4-}$ (x = 0.82) was obtained by using 0.7−0.9 mol of $POCl_3$ per mole of $[NEt_4]_2[Ni_6(CO)_{12}]^{2-}$ in CH_3CN or thf. In the latter case, $[Ni_{22}P_6(CO)_{30}]^{2-}$ was also observed as a side product. Details on the syntheses and characterizations of the new clusters $[Ni_{14}P_2(CO)_{22}]^{2-}$, $[Ni_{22-x}P_2(CO)_{29-x}]^{4-}$ (x = 0.84), $[Ni_{39}P_3(CO)_{44}]^{6-}$, $[Ni_{23-x}P_2(CO)_{30-x}]^{4-}$ (x = 0.82), and $[Ni_{22}P_6(CO)_{30}]^{2-}$ are reported in the following sections.

Synthesis and Molecular Structure of $[Ni_{14}P_2(CO)_{22}]^{2-}$. The reaction of $[Ni_6(CO)_{12}]^{2-}$ as a $[NBu_4]^+$ salt in CH_2Cl_2 with PCl_3 afforded $[NBu_4]_2[Ni_{14}P_2(CO)_{22}]$ as an oily precipitate. $Ni(CO)_4$ was formed as a side product, as inferred by IR spectroscopy, and eliminated in a vacuum. The solid residue was recovered after filtration and washed with H_2O and $[Ni_{14}P_2(CO)_{22}]^{2-}$ extracted in CH_2Cl_2. Crystals of $[NBu_4]_2[Ni_{14}P_2(CO)_{22}]$ suitable for SC-XRD were grown by slow diffusion of n-hexane pn the CH_2Cl_2 solution. Two different polymorphs of $[NBu_4]_2[Ni_{14}P_2(CO)_{22}]$ were obtained (monoclinic $P2_1/n$ and monoclinic $C2/c$).

Crystals of $[NBu_4]_2[Ni_{14}P_2(CO)_{22}]$ displayed ν_{CO} at 2032(s) and 1862(m) cm^{-1} in CH_2Cl_2 solution and ν_{CO} at 2025(s) and 1863(m) cm^{-1} in CH_3CN solution.

The metal cage of $[Ni_{14}P_2(CO)_{22}]^{2-}$ consists of two monocapped P-centered square-antiprismatic Ni_9P units fused through a common square face (Figure 1, Table 1). A similar environment was displayed by two P atoms within the larger $[H_{6-n}Ni_{31}P_4(CO)_{39}]^{n-}$ (n = 4, 5) cluster,[22] whereas the other two P atoms were encapsulated within $Ni_{10}P$ bicapped square antiprisms. Conversely, $[Ni_{11}P(CO)_{18}]^{3-}$ presents a $Ni_{10}P$ sphenocorona cage. It should be noticed that square-antiprismatic cages (with the possibility of capping atoms) were previously found in the case of fully interstitial carbonyl monophosphide clusters of Ru, Rh, and Co.[23−28] A monocapped square-antiprismatic environment was found also in the Ni_3P phase.[1−3]

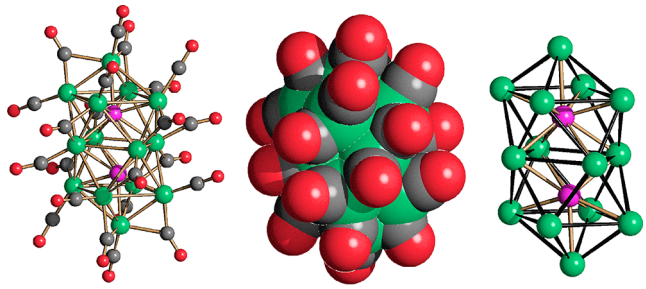

Figure 1. (a) The molecular structure of $[Ni_{14}P_2(CO)_{22}]^{2-}$; (b) its space-filling model; (c) the $Ni_{14}P_2$ core (Ni, green; P, purple; C, gray; O, red). The Ni−Ni bonds of the Ni_{14} cage are represented in black in c.

Table 1. Main Bond Distances (Å) of $[Ni_{14}P_2(CO)_{22}]^{2-}$, $[Ni_{23-x}P_2(CO)_{30-x}]^{4-}$, $[Ni_{22-x}P_2(CO)_{29-x}]^{4-}$, $[Ni_{22}P_6(CO)_{30}]^{2-}$, and $[Ni_{39}P_3(CO)_{44}]^{3-}$

	Ni−Ni	Ni−P	P···P
$[Ni_{14}P_2(CO)_{22}]^{2-,a}$	2.4242(9)−3.0530(10)	2.1976(14)−2.5308(13)	2.641(2)
	average 2.689(4)	average 2.294(4)	
$[Ni_{14}P_2(CO)_{22}]^{2-,b}$	2.4248(17)−3.051(2)	2.204(3)−2.547(3)	2.664(5)
	average 2.691(8)	average 2.295(9)	
$[Ni_{23-x}P_2(CO)_{30-x}]^{4-}$	2.3254(11)−2.8235(11)	2.1681(19)−2.5117(18)	
	average 2.591(9)	average 2.332(8)	
$[Ni_{22-x}P_2(CO)_{29-x}]^{4-}$	2.280(14)−2.963(3)	2.119(4)−2.446(4)	
	average 2.60(2)	average 2.296(16)	
$[Ni_{22}P_6(CO)_{30}]^{2-}$	2.448(3)−2.869(4)	2.200(4)−2.394(4)	
	average 2.61(2)	average 2.29(2)	
$[Ni_{39}P_3(CO)_{44}]^{3-}$	2.312(3)−2.8733(16)	2.291(3)−2.678(2)	
	average 2.584(12)	average 2.452(7)	

[a]As found in $[NBu_4]_2[Ni_{14}P_2(CO)_{22}]$, $P2_1/n$. [b]As found in $[NBu_4]_2[Ni_{14}P_2(CO)_{22}]$, $C2/c$.

The Ni−Ni [2.4242(9)−3.0530(10) Å, average 2.689(4) Å for polymorph $P2_1/n$; 2.4248(17)−3.051(2) Å, average 2.691(8) Å for polymorph $C2/c$] and Ni−P [2.1976(14)−2.5308(13) Å, average 2.294(4) Å for polymorph $P2_1/n$; 2.204(3)−2.547(3) Å, average 2.295(9) Å for polymorph $C2/c$] bonding distances are similar to other Ni−P carbonyl clusters.[22] The P···P contact [2.641(2) Å for polymorph $P2_1/n$; 2.664(5) Å for polymorph $C2/c$] is essentially nonbonding. Indeed, the covalent and van der Waals radii of phosphorus are 1.11 and 1.80 Å, respectively.[36] The cluster contains 22 carbonyl ligands, 10 in terminal and 14 in edge bridging positions.

The cluster possesses 196 cluster valence electrons [CVE; 14 × 10 (Ni) + 5 × 2 (P) + 22 × 2 (CO) + 2 (charge)] which correspond to $6n$ + 14 cluster molecular orbitals (CMOs). This electron count is in accord with the Mingos fused formalism, since the cluster results from two monocapped square-antiprisms (130 CVE based on Wade-Mingos rules) fused through a square face (64 CVE): 130 × 2 − 64 = 196

https://dx.doi.org/10.1021/acs.inorgchem.0c02572
Inorg. Chem. 2020, 59, 16016−16026

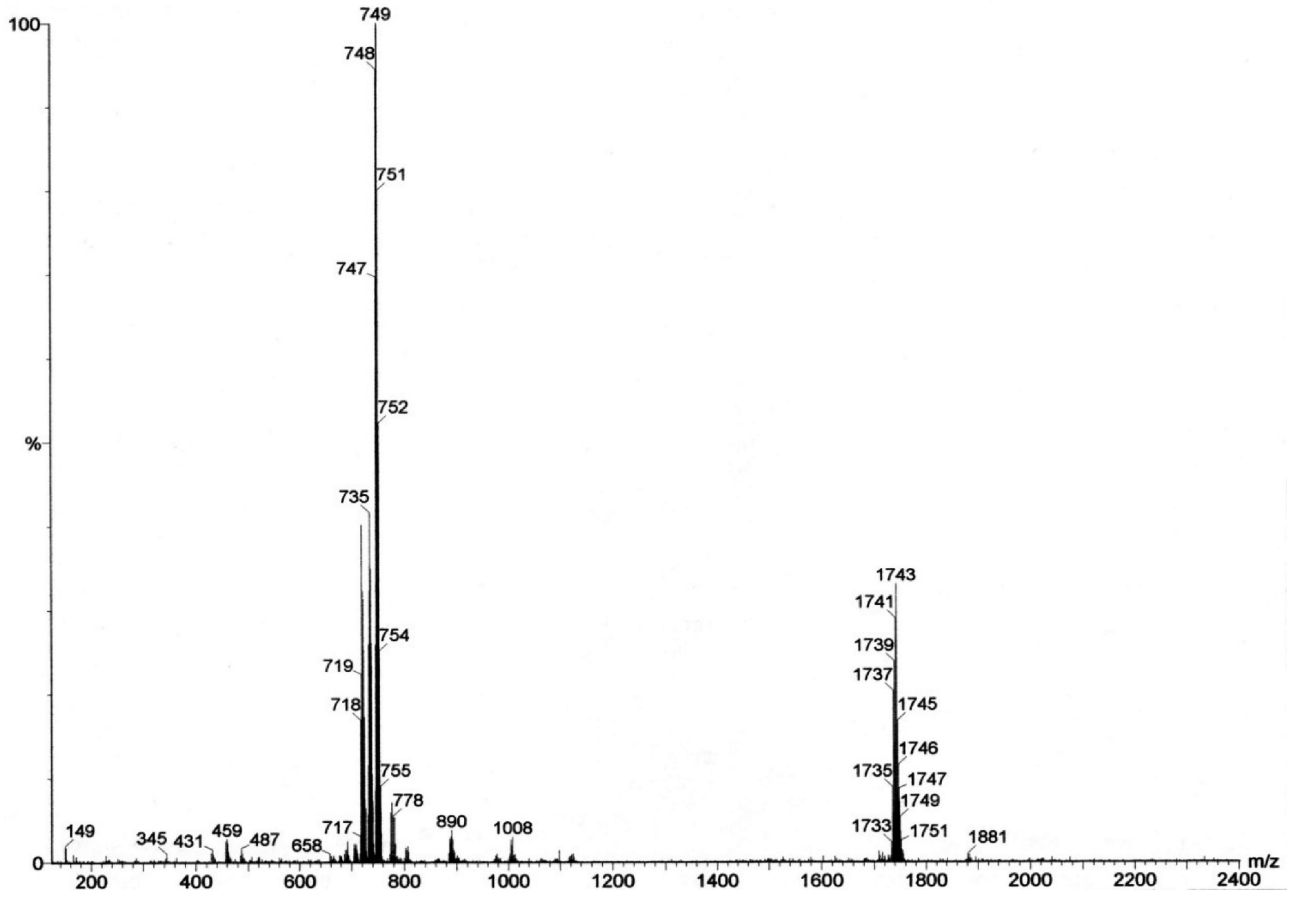

Figure 2. ESI-MS spectrum in CH_3CN (ES−) of $[NBu_4]_2[Ni_{14}P_2(CO)_{22}]$.

CVE.[37] For comparison, both the monocapped square antiprismatic clusters $[Ni_9C(CO)_{17}]^{2-}$[38] and $[Rh_9P(CO)_{21}]^{2-}$[27] possess 130 CVE.

The ESI-MS spectrum of $[Ni_{14}P_2(CO)_{22}]^{2-}$ in CH_3CN solution is reported in Figure 2. The strongest peak at m/z 749 corresponds to the molecular ion $[Ni_{14}P_2(CO)_{22}]^{2-}$ confirming the fact that the cluster fully retains its nature in solution. The dianionic charge of the cluster is further corroborated by the stepwise loss of 14 uma corresponding to a CO ligand (peaks at m/z 735 and 721) for a dianionic species. Finally, the peak at m/z 1743 is due to the $\{[Ni_{14}P_2(CO)_{22}][NBu_4]\}^-$ adduct.

$[Ni_{14}P_2(CO)_{22}]^{2-}$ is poorly stable in solution for a prolonged time. Indeed, while attempting to record its $^{31}P\{^1H\}$ NMR spectrum overnight, several resonances appeared in the range 100−550 ppm, suggesting extended decomposition (Figure S1 in Supporting Information). It must be remarked that phosphorus resonances of interstitial phosphide in metal carbonyl clusters are reported in a very large chemical-shift range, that is, 88−775 ppm.[27,30,39−41] The IR spectrum recorded after the overnight $^{31}P\{^1H\}$ NMR spectrum is rather broad, in keeping with the presence of a mixture of decomposition products. The ν_{CO} bands (2005(s), 1863(ms) cm^{-1}) are indicative of larger clusters, suggesting that the decomposition of $[Ni_{14}P_2(CO)_{22}]^{2-}$ involves some condensation processes. Unfortunately, it has not been possible to isolate and structurally characterize such products.

Synthesis and Molecular Structures of $[Ni_{23-x}P_2(CO)_{30-x}]^{4-}$ (x = 0.82) and $[Ni_{22}P_6(CO)_{30}]^{2-}$. The new cluster $[Ni_{23-x}P_2(CO)_{30-x}]^{4-}$ (x = 0.82) was obtained from the reaction of $[NEt_4]_2[Ni_6(CO)_{12}]$ with 0.7−0.9 equiv of $POCl_3$ in CH_3CN or thf. The formation of $[Ni_{23-x}P_2(CO)_{30-x}]^{4-}$ (x = 0.82) was accompanied by traces of the new $[Ni_{22}P_6(CO)_{30}]^{2-}$ cluster. The two species were separated since $[Ni_{22}P_6(CO)_{30}]^{2-}$ was soluble in thf, whereas $[Ni_{23-x}P_2(CO)_{30-x}]^{4-}$ (x = 0.82) was soluble in acetone.

At the end of the reaction, $Ni(CO)_4$ was eliminated under a vacuum, the Ni(II) salts washed with water, traces of $[Ni_{22}P_6(CO)_{30}]^{2-}$ extracted in thf, and eventually, $[Ni_{23-x}P_2(CO)_{30-x}]^{4-}$ (x = 0.82) extracted in acetone. Crystals of $[NEt_4]_4[Ni_{23-x}P_2(CO)_{30-x}]\cdot 2CH_3COCH_3$ (x = 0.82) suitable for X-ray crystallography were obtained by slow diffusion of n-hexane on the acetone solution (Figure 3, Table 1). Crystals of the $[NEt_4]_2[Ni_{22}P_6(CO)_{30}]\cdot 2thf$ side product were obtained by slow diffusion of n-hexane on the thf solution (Figure 4, Table 1).

$[Ni_{23-x}P_2(CO)_{30-x}]^{4-}$ (x = 0.82) and $[Ni_{22}P_6(CO)_{30}]^{2-}$ are not stable under ESI-MS conditions (Figure S2 in Supporting Information), as often found for larger metal carbonyl clusters, especially in the presence of first-row transition metals such as Ni.

Crystals of $[NEt_4]_4[Ni_{23-x}P_2(CO)_{30-x}]\cdot 2CH_3COCH_3$ (x = 0.82) display ν_{CO} at 2004(s) and 1865(ms) cm^{-1} in CH_3CN solution. Crystals of $[NEt_4]_2[Ni_{22}P_6(CO)_{30}]\cdot 2thf$ display ν_{CO} at 2031(vs), 1943(w), and 1836(m) cm^{-1} in thf solution. Due to the reduced negative charge, the ν_{CO} bands of $[NEt_4]_2[Ni_{22}P_6(CO)_{30}]\cdot 2thf$ are considerably shifted toward higher wavenumbers compared to $[NEt_4]_4[Ni_{23-x}P_2(CO)_{30-x}]\cdot 2CH_3COCH_3$.

https://dx.doi.org/10.1021/acs.inorgchem.0c02572
Inorg. Chem. 2020, 59, 16016−16026

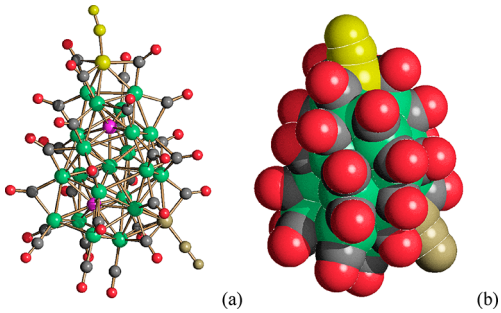

Figure 3. (a) The molecular structure of $[Ni_{23-x}P_2(CO)_{30-x}]^{4-}$ (x = 0.82) and (b) its space-filling model (Ni, green; P, purple; C, gray; O, red). The Ni(CO) fragment with 0.50 occupancy factor is represented in yellow. The Ni(CO) fragment with 0.68 occupancy factor is represented in olive green.

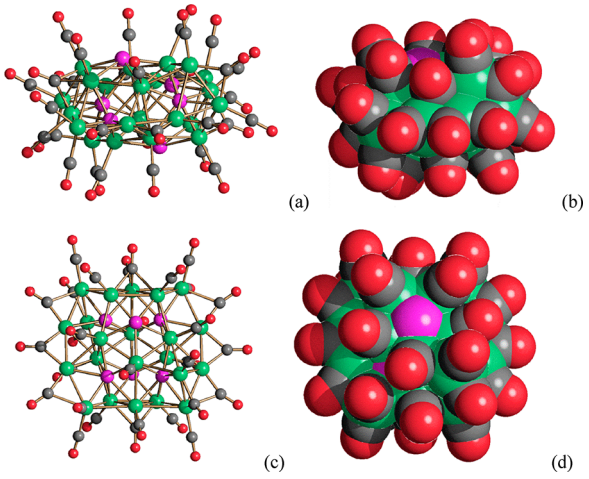

Figure 4. (a,c) Two views of the molecular structure of $[Ni_{22}P_6(CO)_{30}]^{2-}$ and (b,d) its space-filling model (Ni, green; P, purple; C, gray; O, red).

The $Ni_{22}P_2$ cage present in $[Ni_{23-x}P_2(CO)_{30-x}]^{4-}$ (x = 0.82) is composed of one distorted Ni_9P monocapped square antiprism (Ni atoms in green, Ni−Ni bonds in red, Ni−P bonds in yellow in Figure 5) and one distorted $Ni_{10}P$ sphenocorona (Ni atoms in orange, Ni−Ni bonds in blue, Ni−P bonds in green) fused together through a common vertex (in blue in Figure 5). This results in a $Ni_{18}P_2$ framework which can be completed by the addition of four further Ni atoms not bonded to any P. Three of these Ni atoms (in cyan in Figure 5) have full occupancy factors, whereas the fourth (in olive green in Figure 5) shows a refined 0.68 occupancy factor. Capping a triangular face of this $Ni_{22}P_2$ cage with an additional Ni atom (in yellow in Figure 5; 0.50 occupancy factor) affords the final $Ni_{23}P_2$ metal framework of $[Ni_{23}P_2(CO)_{30}]^{4-}$.

Thus, $[Ni_{23-x}P_2(CO)_{30-x}]^{4-}$ (x = 0.82) contains two Ni(CO) fragments with partial occupancy factors (0.68 and 0.50, respectively). This experimental disorder may be interpreted by two different models: (a) $[Ni_{23-x}P_2(CO)_{30-x}]^{4-}$ (x = 0.82) is actually a mixture of $[Ni_{23}P_2(CO)_{30}]^{4-}$ (18%) and two isomers of $[Ni_{22}P_2(CO)_{29}]^{4-}$ (82%); (b) $[Ni_{23-x}P_2(CO)_{30-x}]^{4-}$ (x = 0.82) is actually a mixture of $[Ni_{23}P_2(CO)_{30}]^{4-}$ (34%), two isomers of $[Ni_{22}P_2(CO)_{29}]^{4-}$ (34% and 16%, respectively), and $[Ni_{21}P_2(CO)_{28}]^{4-}$ (16%). On the basis of SC-XRD data, it is not possible to distinguish between these two models. Nonetheless, in both cases, it is possible to conclude that $[Ni_{23-x}P_2(CO)_{30-x}]^{4-}$ (x = 0.82) is mainly composed of $[Ni_{22}P_2(CO)_{29}]^{4-}$ (50−82%) which consists of two isomers differing in the positions of a Ni(CO) fragment. The contemporary presence of both these Ni(CO) fragments results in $[Ni_{23}P_2(CO)_{30}]^{4-}$, whereas $[Ni_{21}P_2(CO)_{28}]^{4-}$ results when they are both absent. This phenomenon is well-known for Ni carbonyl clusters, and indeed, several species differing for the addition/subtraction of a few Ni(CO) fragments have been reported.[42−44]

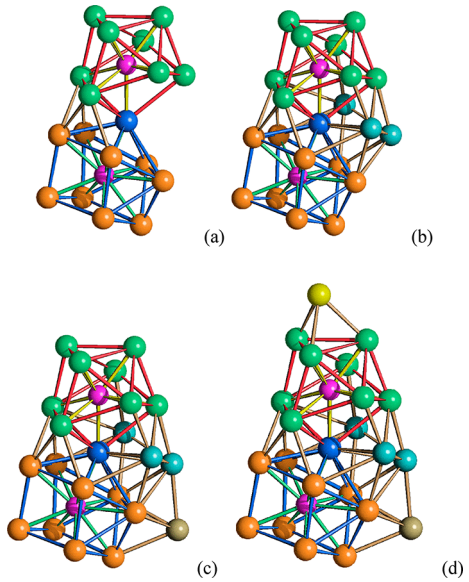

Figure 5. Formal building-up of the metal cage of $[Ni_{23-x}P_2(CO)_{30-x}]^{4-}$ (x = 0.82) (P atoms are represented in purple). (a) The $Ni_{18}P_2$ framework obtained by the condensation via a vertex (in blue) of a Ni_9P monocapped square antiprism (Ni atoms in green, Ni−Ni bonds in red, Ni−P bonds in yellow) and a $Ni_{10}P$ sphenocorona (Ni atoms in orange, Ni−Ni bonds in blue, Ni−P bonds in green). (b) The $Ni_{21}P_2$ core of $[Ni_{21}P_2(CO)_{28}]^{4-}$ (cyan, additional Ni atoms not bonded to P). (c) The $Ni_{22}P_2$ core of $[Ni_{22}P_2(CO)_{29}]^{4-}$ (olive green, capping Ni with 0.68 occupancy factor). (d) The $Ni_{23}P_2$ core of $[Ni_{23}P_2(CO)_{30}]^{4-}$ (yellow, capping Ni with 0.50 occupancy factor).

The cluster contains one fully interstitial Ni atom (in blue in Figure 5), 67 Ni−Ni bonding contacts (64 and 63 for the two isomers of $[Ni_{22}P_2(CO)_{29}]^{4-}$; 60 for $[Ni_{21}P_2(CO)_{28}]^{4-}$), and 19 Ni−P interactions. The interstitial Ni atom displays 11 Ni−Ni and two Ni−P contacts. The $[Ni_{23}P_2(CO)_{30}]^{4-}$ cluster is completed by 30 CO ligands, seven terminal, 19 edge bridging, and four face capping. $[Ni_{22}P_2(CO)_{29}]^{4-}$ contains 29 CO ligands: nine terminal, 16 edge bridging, and four face capping in the case of the first isomer (yellow Ni(CO) fragment, as depicted in Figure 5, is missing); seven terminal, 20 edge bridging, and two face capping in the case of the second isomer (olive green Ni(CO) fragment, as depicted in Figure 5, is missing). $[Ni_{21}P_2(CO)_{28}]^{4-}$ contains 28 CO ligands, nine terminal, 17 edge bridging, and two face capping.

On the basis of the capping principle, $[Ni_{23}P_2(CO)_{30}]^{4-}$ (304 CVE), $[Ni_{22}P_2(CO)_{29}]^{4-}$ (292 CVE), and $[Ni_{21}P_2(CO)_{28}]^{4-}$ (280 CVE) have analogous electron counts which correspond to $6n$ + 14 CMO, as found also in $[Ni_{14}P_2(CO)_{22}]^{2-}$.

The $^{31}P\{^1H\}$ NMR spectrum of $[Ni_{23-x}P_2(CO)_{30-x}]^{4-}$ (x = 0.82) in CD_3CN displays four resonances at δ_P 470, 338, 288, and 212 ppm (Figure 6). These resonances are very broad,

https://dx.doi.org/10.1021/acs.inorgchem.0c02572
Inorg. Chem. 2020, 59, 16016−16026

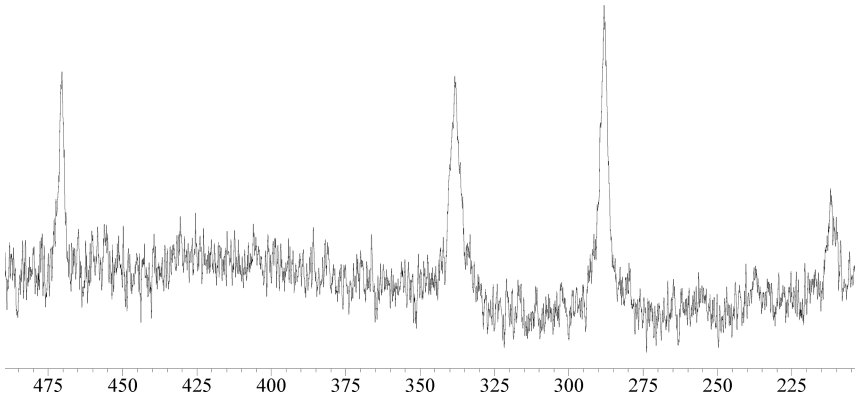

Figure 6. $^{31}P\{^{1}H\}$ NMR spectrum of $[Ni_{23-x}P_2(CO)_{30-x}]^{4-}$ (x = 0.82) in CD_3CN at 298 K.

hampering a reliable integration of the spectrum. The weakest resonance at 212 ppm might be due to impurities or to a minor species of the $[Ni_{23-x}P_2(CO)_{30-x}]^{4-}$ (x = 0.82) mixture. Nonetheless, the presence of 3−4 resonances is in agreement with the fact that $[Ni_{23-x}P_2(CO)_{30-x}]^{4-}$ (x = 0.82) is actually a mixture of species differing for the presence and/or position of a few Ni(CO) groups (see above).

Two views of the molecular structure of $[Ni_{22}P_6(CO)_{30}]^{2-}$ are reported in Figure 4, whereas the formal building up of its $Ni_{22}P_6$ cage is represented in Figure 7. The core of the cluster

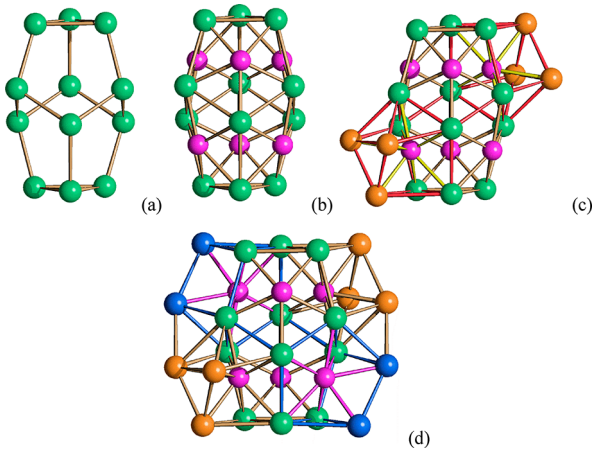

Figure 7. Formal building up of the metal cage of $[Ni_{22}P_6(CO)_{30}]^{2-}$. (a) The Ni_{12} polyhedron of pseudo-D_{3d} symmetry with two triangular and six pentagonal faces (green, Ni). (b) The $Ni_{12}P_6$ core obtained by adding six P atoms on the six pentagonal faces (purple, P). (c) The $Ni_{18}P_6$ framework obtained by capping two P atoms within two distorted bicapped trigonal prismatic cages (additional Ni in orange; Ni−Ni and Ni−P bonds of the bicapped trigonal prismatic cages are highlighted in red and yellow, respectively). (d) The $Ni_{22}P_6$ cage obtained by partially capping two P atoms within two distorted monocapped trigonal prismatic cages (additional Ni in blue; Ni−Ni and Ni−P bonds of the monocapped trigonal prismatic cages are highlighted in blue and purple, respectively).

consists of a Ni_{12} polyhedron of *pseudo* D_{3d} symmetry, which possesses two parallel triangular and six adjacent pentagonal faces. The six P atoms are capping the six pentagonal faces, resulting in a $Ni_{12}P_6$ cage. The environments of these six P atoms are rather different: (a) Two P atoms are exposed on the cluster surface, being connected only to the five Ni atoms of the pentagonal face. (b) Two P atoms are fully interstitial, being encapsulated within distorted Ni_8P bicapped trigonal prismatic cages, obtained by adding three further Ni atoms per P atom (in orange in Figure 7). (c) Two P atoms are in semi-interstitial positions within highly distorted Ni_7P monocapped trigonal prismatic cages, resulting from the addition of two further Ni atoms per P atom (in blue in Figure 7).

The $[Ni_{22}P_6(CO)_{30}]^{2-}$ cluster possesses 30 CO ligands, 22 terminal, six edge bridging, and two face capping. The cluster displays 312 CVEs, corresponding to $6n$ + 24 CMOs, by considering all six P atoms as contributing with five electrons each. Conversely, by considering the two exposed P atoms contributing with only three electrons to the electron count, the cluster possesses 308 CVEs and $6n$ + 22 CMOs. In both cases, $[Ni_{22}P_6(CO)_{30}]^{2-}$ is rather electron rich, as often found in larger Ni carbonyl clusters containing several interstitial heteroatoms.[45−47] Indeed, the electron count of Ni−P carbonyl clusters seems to increase considerably by increasing the number of P atoms, that is, $[Ni_{11}P(CO)_{18}]^{3-}$ ($6n$ + 11), $[Ni_{14}P_2(CO)_{22}]^{2-}$ ($6n$ + 14), $[Ni_{23-x}P_2(CO)_{29-x}]^{4-}$ ($6n$ + 14), $[Ni_{39}P_3(CO)_{44}]^{6-}$ ($6n$ + 16), $[HNi_{31}P_4(CO)_{34}]^{5-}$ ($6n$ + 21), and $[Ni_{22}P_6(CO)_{30}]^{2-}$ ($6n$ + 22 or $6n$ + 24).

In agreement with the solid state structure, the $^{31}P\{^{1}H\}$ NMR spectrum of $[Ni_{22}P_6(CO)_{30}]^{2-}$ in CD_3CN displays three equally intense resonances at δ_P 503.2, 401.4, and 383.6 ppm (Figure S3 in Supporting Information). These resonances show some fine structures likely due to a larger and a smaller coupling constant, that is J_{PP} = 90 and 30 Hz, respectively.

Synthesis and Molecular Structure of $[Ni_{22-x}P_2(CO)_{29-x}]^{4-}$ (x = 0.84). $[Ni_{22-x}P_2(CO)_{29-x}]^{4-}$ (x = 0.84) resulted from the reaction of $[NEt_4]_2[Ni_6(CO)_{12}]$ with 0.4−0.5 equiv of $POCl_3$ in CH_3CN. At the end of the reaction, $Ni(CO)_4$ was removed in a vacuum. The Ni(II) salts were washed with H_2O. Traces of $[Ni_6(CO)_{12}]^{2-}$ were extracted in thf, and eventually, $[Ni_{22-x}P_2(CO)_{29-x}]^{4-}$ (x = 0.84) was extracted in acetone. Crystals of $[NEt_4]_4[Ni_{22-x}P_2(CO)_{29-x}]\cdot 2CH_3COCH_3$ (x = 0.84) suitable for SC-XRD were obtained by slow diffusion of *n*-hexane on the acetone solutions (Figure 8, Table 1).

Crystals of $[NEt_4]_4[Ni_{22-x}P_2(CO)_{29-x}]\cdot 2CH_3COCH_3$ (x = 0.84) display ν_{CO} at 2003(vs), 1962(sh), and 1869(s) cm^{-1} in CH_3CN. The crystals actually contain a mixture of $[Ni_{22}P_2(CO)_{29}]^{4-}$ (16%) and $[Ni_{21}P_2(CO)_{28}]^{4-}$ (84%), since there is a Ni(CO) fragment with 0.16 refined occupancy factor (in yellow in Figure 8). In agreement with the presence of a mixture of two products (a major one and a minor one), the $^{31}P\{^{1}H\}$ NMR spectrum shows two broad resonances at δ_P 212.9 and 163.8 ppm (Figure S4 in Supporting Information). As in the case of $[Ni_{23-x}P_2(CO)_{30-x}]^{4-}$ (x = 0.82),

https://dx.doi.org/10.1021/acs.inorgchem.0c02572
Inorg. Chem. 2020, 59, 16016−16026

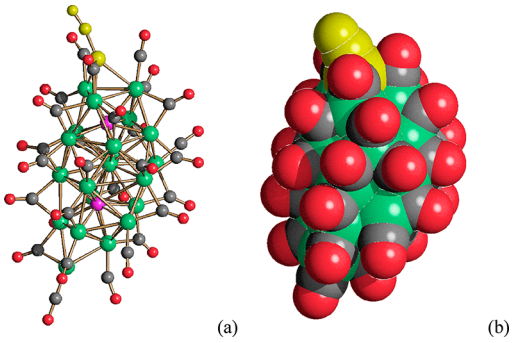

Figure 8. (a) The molecular structure of $[Ni_{22-x}P_2(CO)_{29-x}]^{4-}$ (x = 0.84) and (b) its space-filling model (Ni, green; P, purple; C, gray; O, red). The Ni(CO) fragment with a partial occupancy factor is represented in yellow.

$[Ni_{22-x}P_2(CO)_{29-x}]^{4-}$ (x = 0.84) was not stable under ESI-MS conditions.

Despite the fact that $[Ni_{22-x}P_2(CO)_{29-x}]^{4-}$ (x = 0.84) and $[Ni_{23-x}P_2(CO)_{30-x}]^{4-}$ (x = 0.82) have very similar formulas, they display significantly different metal cages, which might be viewed as isomers. Structural isomerism in molecular clusters of increasing sizes is rather interesting in view of its relevance to the field of metal nanoclusters, nanoparticles, and nanomaterials.[48−52]

The main difference between $[Ni_{22-x}P_2(CO)_{29-x}]^{4-}$ (x = 0.84) and $[Ni_{23-x}P_2(CO)_{30-x}]^{4-}$ (x = 0.82) consists of the fact that the former results from one distorted Ni_9P monocapped square antiprism, as $[Ni_{23-x}P_2(CO)_{30-x}]^{4-}$ (x = 0.5), and one distorted $Ni_{10}P$ bicapped square antiprism, rather than a $Ni_{10}P$ sphenocorona. These two cages are fused together through a common vertex (Figure 9), resulting in a $Ni_{18}P_2$ framework

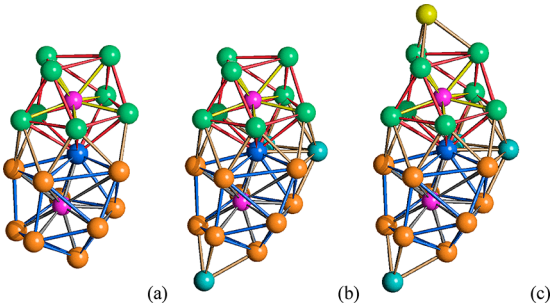

Figure 9. Formal building-up of the metal cage of $[Ni_{22-x}P_2(CO)_{29-x}]^{4-}$ (x = 0.84) (P atoms are represented in purple). (a) The $Ni_{18}P_2$ framework obtained by the condensation via a vertex (in blue) of a Ni_9P monocapped square antiprism (Ni atoms in green, Ni−Ni bonds in red, Ni−P bonds in yellow) and a $Ni_{10}P$ bicapped square antiprism (Ni atoms in orange, Ni−Ni bonds in blue, Ni−P bonds in gray). (b) The $Ni_{21}P_2$ core of $[Ni_{21}P_2(CO)_{28}]^{4-}$ (cyan, additional Ni atoms not bonded to P). (c) The $Ni_{22}P_2$ core of $[Ni_{22}P_2(CO)_{29}]^{4-}$ (yellow, capping Ni with partial occupancy factor).

which may be viewed as an isomer of the $Ni_{18}P_2$ framework present in $[Ni_{23-x}P_2(CO)_{30-x}]^{4-}$ (x = 0.82). The $Ni_{21}P_2$ cage of $[Ni_{22-x}P_2(CO)_{29-x}]^{4-}$ (x = 0.84) is completed by the addition of three further Ni atoms not bonded to any P. Capping a triangular face of this with an additional Ni atoms affords the final $Ni_{22}P_2$ metal framework of $[Ni_{22}P_2(CO)_{29}]^{4-}$.

The cluster contains one fully interstitial Ni atom (in blue in Figure 9), 63 Ni−Ni bonding contacts (60 for $[Ni_{21}P_2(CO)_{28}]^{4-}$), and 19 Ni−P interactions. The interstitial Ni atom displays 12 Ni−Ni and two Ni−P contacts. The $[Ni_{22}P_2(CO)_{29}]^{4-}$ cluster is completed by 29 CO ligands, four terminal and 25 edge bridging. Conversely, $[Ni_{21}P_2(CO)_{28}]^{4-}$ contains 28 CO ligands, six terminal and 22 edge bridging.

The electron count of the $[Ni_{22}P_2(CO)_{29}]^{4-}$ (292 CVE) and $[Ni_{21}P_2(CO)_{28}]^{4-}$ (280 CVE) clusters found in $[Ni_{22-x}P_2(CO)_{29-x}]^{4-}$ (x = 0.84) corresponds to $6n$ + 14 CMO, as in the case of $[Ni_{23-x}P_2(CO)_{30-x}]^{4-}$ (x = 0.82).

Synthesis and Molecular Structure of $[Ni_{39}P_3(CO)_{44}]^{6-}$. $[Ni_{39}P_3(CO)_{44}]^{6-}$ was obtained following a very similar procedure to that described for the synthesis of $[Ni_{22-x}P_2(CO)_{29-x}]^{4-}$ (x = 0.84) but performing the reaction in thf rather than CH_3CN. Thus, $[NEt_4]_2[Ni_6(CO)_{12}]$ was reacted with 0.4−0.5 equiv of $POCl_3$ in thf, and after workup, $[Ni_{39}P_3(CO)_{44}]^{6-}$ was extracted in CH_3CN. Slow diffusion on n-hexane and di-iso-propyl-ether afforded a few crystals of $[NEt_4]_6[Ni_{39}P_3(CO)_{44}]\cdot C_6H_{14}\cdot$solv suitable for SC-XRD (Figure 10 and Table 1). The compound displays ν_{CO} at 1998(vs) and 1868(s) cm^{-1} in CH_3CN.

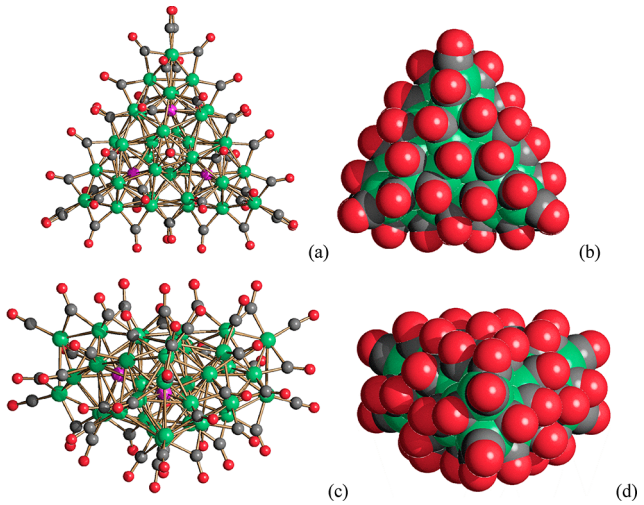

Figure 10. (a,c) The molecular structure of $[Ni_{39}P_3(CO)_{44}]^{6-}$ and (b,d) its space-filling model (Ni, green; P, purple; C, gray; O, red).

The structure of $[Ni_{39}P_3(CO)_{44}]^{6-}$ is based on a $Ni_{39}P_3$ metal core of idealized D_{3h} symmetry and 39 CO ligands, six terminal, 36 edge bridging, and two face capping (Figure 11). The metal core of the cluster is composed of three $Ni_{12}P$ centered icosahedra fused together around a 3-fold axis. Each $Ni_{12}P$ centered icosahedron shares two contiguous Ni atoms with the other two icosahedra, resulting in a $Ni_{33}P_3$ framework. The three Ni atoms shared by the three icosahedra form a fully interstitial Ni_3 triangle. Each Ni atom within this triangle is bonded to 10 Ni atoms and two P atoms. The $Ni_{39}P_3$ core of the cluster is completed by adding three Ni_2 units, one per $Ni_{12}P$ icosahedron. These two additional Ni atoms are capping two adjacent triangular faces within each icosahedron. The additional Ni atoms are not bonded to P, and they are coordinated to the six terminal carbonyls present in the cluster.

This represents the first case of a phosphide atom enclosed within an icosahedral cage in a transition metal cluster. Indeed, P atoms are usually found in smaller cages with coordination numbers comprised in the range 5−10.[22−30,40,41,53−56] Icosahedra are often found with larger heteroatoms, such as Sn, Sb, Bi, and Ge.[57,58]

https://dx.doi.org/10.1021/acs.inorgchem.0c02572
Inorg. Chem. 2020, 59, 16016−16026

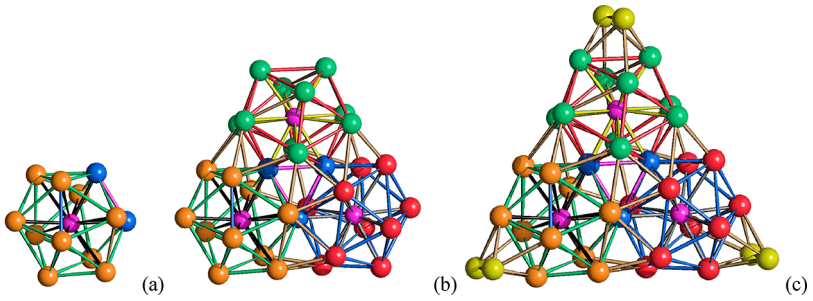

Figure 11. Formal building-up of the metal cage of $[Ni_{39}P_3(CO)_{44}]^{6-}$ (P atoms are represented in purple). (a) One of the three P-centered $Ni_{12}P$ icosahedra (Ni atoms belonging only to this icosahedron in orange, Ni atoms shared with other icosahedra in blue, Ni−Ni bonds in green, Ni−P bonds in black). (b) The $Ni_{33}P_3$ core obtained by fusing three $Ni_{12}P$ icosahedra sharing three atoms (different colors have been used for the Ni atoms, Ni−Ni and Ni−P bonds within each icosahedron; the shared Ni_3 triangle is represented in blue, its Ni−Ni bonds in purple). (c) The $Ni_{39}P_3$ core of $[Ni_{39}P_3(CO)_{44}]^{6-}$ obtained after the addition of three Ni_2 units, one per each icosahedron (yellow, additional Ni atoms not bonded to P).

CONCLUSIONS

Five new molecular nickel phosphide carbonyl clusters, that is, $[Ni_{14}P_2(CO)_{22}]^{2-}$, $[Ni_{22-x}P_2(CO)_{29-x}]^{4-}$ (x = 0.84), $[Ni_{39}P_3(CO)_{44}]^{6-}$, $[Ni_{23-x}P_2(CO)_{30-x}]^{4-}$ (x = 0.82), and $[Ni_{22}P_6(CO)_{30}]^{2-}$, have been structurally characterized, and they add to the previously reported $[Ni_{11}P(CO)_{18}]^{3-}$ and $[H_{6-n}Ni_{31}P_4(CO)_{39}]^{n-}$ (n = 4, 5). The sizes of the metal cores of these clusters range from 0.59 to 1.10 nm, and their overall dimensions including the CO ligands are 1.16−1.63 nm (Table 2). Thus, the sizes of these molecular clusters are comparable

Table 2. Dimensions of the Known Ni−P−CO Molecular Clusters

	metal core	size including CO
$[Ni_{11}P(CO)_{18}]^{3-}$	0.59 nm	1.16 nm
$[Ni_{14}P_2(CO)_{22}]^{2-}$	0.72 nm	1.23 nm
$[Ni_{22}P_6(CO)_{30}]^{2-}$	0.99 nm	1.40 nm
$[Ni_{23-x}P_2(CO)_{30-x}]^{4-}$ (x = 0.82)	0.98 nm	1.54 nm
$[Ni_{22-x}P_2(CO)_{29-x}]^{4-}$ (x = 0.84)	1.08 nm	1.59 nm
$[H_{6-n}Ni_{31}P_4(CO)_{39}]^{n-}$ (n = 4, 5)	1.04 nm	1.60 nm
$[Ni_{39}P_3(CO)_{44}]^{6-}$	1.10 nm	1.63 nm

to those of ultrasmall metal nanoparticles, molecular nanoclusters, or atomically precise metal nanoparticles.[59−61] In this respect, interstitial phosphide atoms seem to be as effective as carbides in order to stabilize molecular nickel carbonyl nanoclusters.[42−45,59]

The environment of the P atoms within these molecular Ni−P−CO nanoclusters displays a rich diversity. Indeed, they may be fully interstitial, semiexposed, or exposed in very diverse cages, that is, Ni_5P pentagonal pyramid (exposed P in a pentagonal face), (highly distorted) Ni_7P monocapped trigonal prism (semiexposed P), Ni_8P bicapped trigonal prism, Ni_9P monocapped square antiprism, $Ni_{10}P$ sphenocorona, $Ni_{10}P$ bicapped square antiprism, and $Ni_{12}P$ icosahedron (Figure 12).

This structural diversity is paralleled by the richness of structural motives found in Ni−P phases and nanostructures. Indeed, Ni-rich phases show isolated P atoms inside a Ni_9P tricapped trigonal prismatic cage (Ni_2P phase), a distorted Ni_9P monocapped square antiprismatic cage (Ni_3P phase), and a mixture of $Ni_{10}P$ sphenocorona and Ni_9P monocapped cubic cages ($Ni_{12}P_5$ phase). Therefore, some of these structural motives are common to molecular metal carbonyl clusters and solid state Ni−P phases (Ni_9P monocapped square antiprism, $Ni_{10}P$ sphenocorona); some others have been found for the

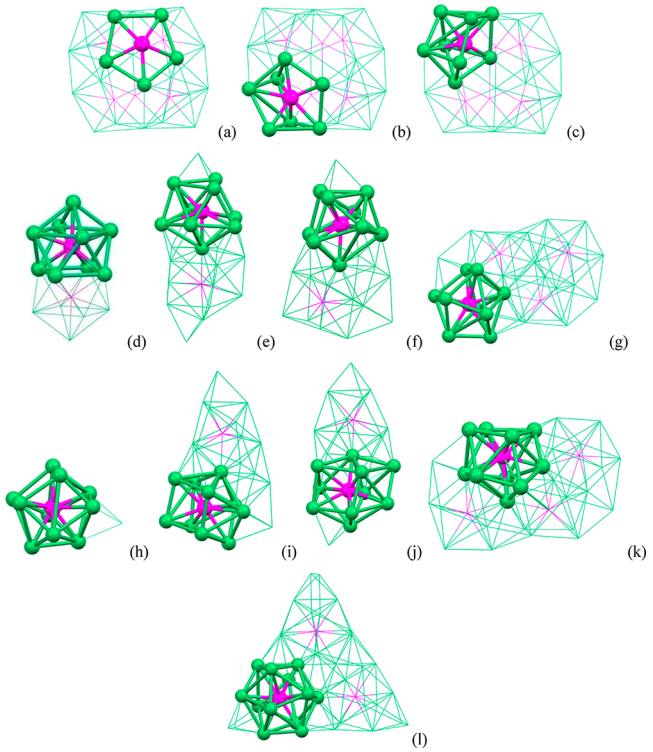

Figure 12. Diverse environments of P atoms in Ni−P−CO clusters. Ni_5P, pentagonal pyramid of (a) $[Ni_{22}P_6(CO)_{30}]^{2-}$; Ni_7P, monocapped trigonal prism of (b) $[Ni_{22}P_6(CO)_{30}]^{2-}$; Ni_8P, bicapped trigonal prism of (c) $[Ni_{22}P_6(CO)_{30}]^{2-}$; Ni_9P, monocapped square antiprism of (d) $[Ni_{14}P_2(CO)_{22}]^{2-}$, (e) $[Ni_{22-x}P_2(CO)_{29-x}]^{4-}$, (f) $[Ni_{23-x}P_2(CO)_{30-x}]^{4-}$, and (g) $[H_{6-n}Ni_{31}P_4(CO)_{39}]^{n-}$ (n = 4, 5); $Ni_{10}P$, sphenocorona of (h) $[Ni_{11}P(CO)_{18}]^{3-}$ and (i) $[Ni_{23-x}P_2(CO)_{30-x}]^{4-}$; $Ni_{10}P$, bicapped square antiprism of (j) $[Ni_{22-x}P_2(CO)_{29-x}]^{4-}$ and (k) $[H_{6-n}Ni_{31}P_4(CO)_{39}]^{n-}$ (n = 4, 5); $Ni_{12}P$, icosahedron of (l) $[Ni_{39}P_3(CO)_{44}]^{6-}$.

moment only in metal carbonyl clusters (Ni_5P pentagonal pyramid, Ni_7P monocapped trigonal prism, Ni_8P bicapped trigonal prism, $Ni_{10}P$ bicapped square antiprism, $Ni_{12}P$ icosahedron) or solely in solid state Ni−P phases (Ni_9P tricapped trigonal prism, Ni_9P monocapped cube). In addition, P-richer solid state Ni−P phases display direct P−P bonds which may result in P_2 units (NiP and the high-pressure cubic NiP_2), zig-zig chains (monoclinic NiP_2), and P_4 units (NiP_3), as well as more complex and less regular structures. In contrast,

https://dx.doi.org/10.1021/acs.inorgchem.0c02572
Inorg. Chem. 2020, 59, 16016−16026

molecular Ni−P carbonyl clusters containing direct P−P interactions have not been isolated yet.

■ ASSOCIATED CONTENT

Supporting Information

The Supporting Information is available free of charge at https://pubs.acs.org/doi/10.1021/acs.inorgchem.0c02572.

NMR spectra, crystals and experimental details, ORTEP drawings of all the structures (PDF)

Accession Codes

CCDC 2025497, 2025498, 2025499, 2025500, 2025501, and 2025502 contain the supplementary crystallographic data for this paper. These data can be obtained free of charge via www.ccdc.cam.ac.uk/data_request/cif, or by emailing data_request@ccdc.cam.ac.uk, or by contacting The Cambridge Crystallographic Data Centre, 12, Union Road, Cambridge CB2 1EZ, UK; fax: + 44 1223 336033.

■ AUTHOR INFORMATION

Corresponding Author

Stefano Zacchini − *Dipartimento di Chimica Industriale "Toso Montanari", Università di Bologna, 40136 Bologna, Italy;* orcid.org/0000-0003-0739-0518; Phone: +39 051 2093711; Email: stefano.zacchini@unibo.it; https://www.unibo.it/sitoweb/stefano.zacchini/en

Authors

Chiara Capacci − *Dipartimento di Chimica Industriale "Toso Montanari", Università di Bologna, 40136 Bologna, Italy*

Cristiana Cesari − *Dipartimento di Chimica Industriale "Toso Montanari", Università di Bologna, 40136 Bologna, Italy*

Cristina Femoni − *Dipartimento di Chimica Industriale "Toso Montanari", Università di Bologna, 40136 Bologna, Italy;* orcid.org/0000-0003-4317-6543

Maria Carmela Iapalucci − *Dipartimento di Chimica Industriale "Toso Montanari", Università di Bologna, 40136 Bologna, Italy*

Federica Mancini − *Dipartimento di Chimica Industriale "Toso Montanari", Università di Bologna, 40136 Bologna, Italy*

Silvia Ruggieri − *Dipartimento di Chimica Industriale "Toso Montanari", Università di Bologna, 40136 Bologna, Italy;* orcid.org/0000-0002-2849-0449

Complete contact information is available at: https://pubs.acs.org/10.1021/acs.inorgchem.0c02572

Notes

The authors declare no competing financial interest.

■ ACKNOWLEDGMENTS

The financial support of MIUR (PRIN 2017 "Nemo" 20173L7W8K) and the University of Bologna is gratefully acknowledged.

■ REFERENCES

(1) Chen, J.-H.; Whitmire, K. H. A structural survey of the binary transition metal phosphides and arsenides of the d-block elements. *Coord. Chem. Rev.* **2018**, *355*, 271−327.

(2) Schmetterer, C.; Vizdal, J.; Ipser, H. A new investigation of the system Ni-P. *Intermetallics* **2009**, *17*, 826−834.

(3) (a) Aronsson, B.; Dale, J.; Risberg, E.; Lamm, O. The crystal structure of Ni_3P (Fe_3P-Type). *Acta Chem. Scand.* **1955**, *9*, 137−140. (b) Rundqvist, S.; Hassler, E.; Lundvik, L.; Motzfeldt, K.; Theander, O.; Flood, H. Refinement of the Ni_3P structure. *Acta Chem. Scand.* **1962**, *16*, 242−243.

(4) (a) Oryshchyn, S.; Babizhetskyy, V.; Chykhriy, S.; Aksel'rud, L.; Stoyko, S.; Bauer, J.; Guérin, R.; Kuz'ma, Yu. Crystal Structure of Ni_5P_2. *Inorg. Mater.* **2004**, *40*, 380−385. (b) Saini, G. S.; Calvert, L. D.; Taylor, J. B. Compounds of the type M_5X_2: Pd_5As_2, Ni_5Si_2, and Ni_5P_2. *Can. J. Chem.* **1964**, *42*, 1511−1517.

(5) (a) Elfstrom, M.; Ranby, B.; Sjoberg, B.; Mellander, O.; Hinton, M. The Crystal Structure of Ni_5P_4. *Acta Chem. Scand.* **1965**, *19*, 1694−1704. (b) Donohue, P. C.; Bither, T. A.; Young, H. S. High-Pressure Synthesis of Pyrite-Type Nickel Diphosphide and Nickel Diarsenide. *Inorg. Chem.* **1968**, *7*, 998−1001.

(6) Prins, R.; Bussell, M. E. Metal Phosphides: Preparation, Characterization and Catalytic Reactivity. *Catal. Lett.* **2012**, *142*, 1413−1436.

(7) Owens-Baird, B.; Kolen'ko, Y. V.; Kovnir, K. Structure-Activity Relationships for Pt-Free Metal Phosphide Hydrogen Evolution Electrocatalysts. *Chem. - Eur. J.* **2018**, *24*, 7298−7311.

(8) Hu, C.; Lv, C.; Liu, S.; Shi, Y.; Song, J.; Zhang, Z.; Cai, J.; Watanabe, A. Nickel Phosphide Electrocatalysts for Hydrogen Evolution Reaction. *Catalysts* **2020**, *10*, 188.

(9) Alexander, A.-M.; Hargreaves, S. J. Alternative catalytic materials: carbides, nitrides, phosphides and amorphous boron alloys. *Chem. Soc. Rev.* **2010**, *39*, 4388−4401.

(10) (a) Whitmire, K. H. Transition metal complexes of the naked pnictide elements. *Coord. Chem. Rev.* **2018**, *376*, 114−195. (b) Whitmire, K. H.; Schipper, D. E. In pursuit of advanced materials from single-source precursors based on metal carbonyls. *Dalton Trans.* **2019**, *48*, 2248−2262.

(11) (a) Ren, J.; Wang, J.-g.; Li, J.-f.; Li, Y.-w. Density functional theory study on crustal nickel phosphides. *J. Fuel Chem. Technol.* **2007**, *35*, 458−464. (b) Popczun, E. J.; McKone, J. R.; Read, C. G.; Biacchi, A. J.; Wiltrout, A. M.; Lewis, N. S.; Schaak, R. E. Nanostructured Nickel Phosphides as an Electrocatalyst for the Hydrogen Evolution Reaction. *J. Am. Chem. Soc.* **2013**, *135*, 9267−9270.

(12) Sawhill, S. J.; Layman, K. A.; Van Wyk, D. R.; Engelhard, M. H.; Wang, C.; Bussell, M. E. Thiophene hydrodesulfurization over nickel phosphide catalysts: effect of the precursor composition and support. *J. Catal.* **2005**, *231*, 300−313.

(13) (a) Pu, Z.; Liu, Q.; Tang, C.; Asiri, A. M.; Sun, X. Ni_2P nanoparticle films supported on a Ti plate as an efficient hydrogen evolution cathode. *Nanoscale* **2014**, *6*, 11031−11034. (b) Kucernak, A. R. J.; Naranammalpuram Sundaram, V. N. Nickel phosphide: the effect of phosphorous content on hydrogen evolution activity and corrosion resistance in acidic medium. *J. Mater. Chem. A* **2014**, *2*, 17435−17445.

(14) Stinner, C.; Tang, Z.; Haouas, M.; Weber, Th; Prins, R. Preparation and ^{31}P NMR Characterization of Nickel Phosphides on Silica. *J. Catal.* **2002**, *208*, 456−466.

(15) Yang, S.; Liang, C.; Prins, R. A novel approach to synthesizing highly active Ni_2P/SiO_2 hydrotrating catalysts. *J. Catal.* **2006**, *237*, 118−130.

(16) Huang, Z.; Chen, Z.; Chen, Z.; Lv, C.; Meng, H.; Zhang, C. $Ni_{12}P_5$ Nanoparticles as an Efficient Catalyst for Hydrogen Generation *via* Electrocatalysis and Photoelectrolysis. *ACS Nano* **2014**, *8*, 8121−8129.

(17) Gan, Y.; Wang, C.; Chen, X.; Liang, P.; Wan, H.; Liu, X.; Tan, Q.; Wu, H.; Rao, H.; Wang, H.; Zhang, J.; Wang, Y.; van Aken, P. A.; Wang, H. High conductivity $Ni_{12}P_5$ nanowires as high-rate electrode material for battery-supercapacitor hybrid devices. *Chem. Eng. J.* **2020**, *392*, 123661.

(18) Zou, X.; Zhang, Y. Noble metal-free hydrogen evolution catalysts for water splitting. *Chem. Soc. Rev.* **2015**, *44*, 5148−5180.

(19) Sun, Y.; Xu, K.; Zhao, Z.; Li, X.; Chen, G.; Li, C. Strongly coupled dual zerovalent nonmetal doped nickel phosphide nanoparticles/N, B-graphene hybrid for pH-Universal hydrogen evolution catalysis. *Appl. Catal., B* **2020**, *278*, 119284.

(20) Liu, X.; Zhao, Y.; Yang, X.; Liu, Q.; Yu, X.; Li, Y.; Tang, H.; Zhang, T. Porous Ni_5P_4 as a promising cocatalyst for boosting the photocatalytic hydrogen evolution reaction performance. *Appl. Catal., B* **2020**, *275*, 119144.
(21) Duan, J.; Chen, S.; Ortiz-Ledon, C. A.; Jaroniec, M.; Qiao, S.-Z. Phosphorus Vacancies that Boost Electrocatalytic Hydrogen Evolution by Two Orders of Magnitude. *Angew. Chem., Int. Ed.* **2020**, *59*, 8181−8186.
(22) Capacci, C.; Ciabatti, I.; Femoni, C.; Iapalucci, M. C.; Funaioli, T.; Zacchini, S.; Zanotti, V. Molecular Nickel Phosphide Carbonyl Nanoclusters: Synthesis, Structure, and Electrochemistry of $[Ni_{11}P(CO)_{18}]^{3-}$ and $[H_{6-n}Ni_{31}P_4(CO)_{39}]^{n-}$ (n = 4 and 5). *Inorg. Chem.* **2018**, *57*, 1136−1147.
(23) (a) Chini, P.; Ciani, G.; Martinengo, S.; Sironi, A.; Longhetti, L.; Heaton, B. T. Synthesis and X-ray crystal structure of the anion $[Co_6(CO)_{14}(\mu\text{-}CO)_2P]^-$; an example of a 'semi-interstitial phosphide'. *J. Chem. Soc., Chem. Commun.* **1979**, 188−189. (b) Ciani, G.; Sironi, A. Crystal and molecular structure of the anion phosphido-di-μ-carbonyltetradecacarbonyl hexacobaltate(1−) in its tetraphenylphosphonium salt. *J. Organomet. Chem.* **1983**, *241*, 385−393.
(24) (a) Hong, C. S.; Berben, L. A.; Long, J. R. Synthesis and characterization of a decacobalt carbonyl cluster with two semi-interstitial phosphorus atoms. *Dalton Trans.* **2003**, 2119−2120. (b) Dreher, C.; Zabel, M.; Bodensteiner, M.; Scheer, M. $[(CO)_4W(PH_3)_2]$ as a Source of Semi-interstitial Phosphorus Ligands in Cobalt Carbonyl Clusters. *Organometallics* **2010**, *29*, 5187−5191.
(25) Ciani, G.; Sironi, A.; Martinengo, S.; Garlaschelli, L.; Della Pergola, R.; Zanello, P.; Laschi, F.; Masciocchi, N. Synthesis and X-ray Characterization of the Phosphido-Carbonyl Cluster Anions $[Co_9(\mu_8\text{-}P)(CO)_{21}]^{2-}$ and $[Co_{10}(\mu_8\text{-}P)(CO)_{22}]^{3-}$. *Inorg. Chem.* **2001**, *40*, 3905−3911.
(26) Ragaini, F.; Sironi, A.; Fumagalli, A. Deactivation of a $[PPN][Rh(CO)_4]$-based catalytic system $[PPN^+ = (PPh_3)_2N^+]$. The first decomposition reaction of PPN^+ and the formation of $[Rh_{10}P(CO)_{22}]^{3-}$. *Chem. Commun.* **2000**, 2117−2118.
(27) (a) Vidal, J. L.; Walker, W. E.; Pruett, R. L.; Schoening, R. C. $[Rh_9P(CO)_{21}]^{2-}$. Example of encapsulation of phosphorus by transition-metal-carbonyl clusters. *Inorg. Chem.* **1979**, *18*, 129−136. (b) Vidal, J. L.; Walker, W. E.; Schoening, R. C. $[Rh_{10}P(CO)_{22}]^{3-}$. A transition-metal carbonyl cluster with a metal polyhedron based on the bicapped square antiprism as illustrated by the structural study of the benzyltriethylammonium salt. *Inorg. Chem.* **1981**, *20*, 238−242.
(28) (a) Randles, M. D.; Willis, A. C.; Cifuentes, M. P.; Humphrey, M. G. High-nuclearity ruthenium carbonyl cluster chemistry. 8: Phosphine activation, CO insertion, and deruthenation at a phosphido cluster − X-ray structures of $[ppn][Ru_8(\mu_8\text{-}P)(\mu\text{-}CO)_2(CO)_{20}]$ and $[ppn][Ru_7(\mu_7\text{-}P)(\mu\text{-}\mu^2\text{-}OCPh)(\mu\text{-}PPh_2)(\mu\text{-}CO)(CO)_{17}]$. *J. Organomet. Chem.* **2007**, *692*, 4467−4472. (b) Cifuentes, M. P.; Waterman, S. M.; Humphrey, M. G.; Heath, G. A.; Skelton, B. W.; White, A. H.; Perera, M. P. S.; Williams, M. L. High nuclearity ruthenium carbonyl clusters chemistry VII. Synthesis, NMR studies, electrochemsitry and X-ray crystal structure of $[PPN][Ru_8(\mu_8\text{-}P)(CO)_{22}]$. *J. Organomet. Chem.* **1998**, *565*, 193−200.
(29) Colbran, S. B.; Housecroft, C. E.; Johnson, B. F. G.; Lewis, J.; Owen, S. M.; Raithby, P. R. An X-ray crystal and electronic structural investigation of the interstitial phosphide cluster $[Os_6(CO)_{18}PCl]$. *Polyhedron* **1988**, *7*, 1759−1765.
(30) (a) Colbran, S. B.; Hay, C. M.; Johnson, B. F. G.; Lahoz, F. J.; Lewis, J.; Raithby, P. R. Synthesis, characterization, and reactivity of transition metal carbonyl clusters containing an interstitial phosphorus in a trigonal co-ordination environment: the X-ray structures of $[PPh_3Me][Os_6(CO)_{18}P]$ and $[Os_6(CO)_{18}P(AuPPh_3)]$. *J. Chem. Soc., Chem. Commun.* **1986**, 1766−1768. (b) Colbran, S. B.; Lahoz, F. J.; Raithby, P. R.; Lewis, J.; Johnson, B. F. G.; Cardin, C. J. Stepwise construction of $[Os_6(CO)_{18}(\mu_6\text{-}P)]^-$, a hexanuclear osmium cluster monoanion with trigonal-prismatic co-ordination for phosphorus: X-ray crystal structures of $[Os_6(\mu\text{-}H)_2(CO)_{20}(MeCN)(\mu_3\text{-}PH)]$ and $[PPh_3Me][Os_6(CO)_{18}(\mu_6\text{-}P)]$. *J. Chem. Soc., Dalton Trans.* **1988**, 173−181.
(31) Longoni, G.; Chini, P.; Cavalieri, A. Carbonylnickelates 1. Synthesis and Chemical Characterization of the $[Ni_5(CO)_{12}]^{2-}$ and $[Ni_6(CO)_{12}]^{2-}$ Dianions. *Inorg. Chem.* **1976**, *15*, 3025−3029.
(32) Keller, E. *SCHAKAL99*; University of Freiburg: Freiburg, Germany, 1999.
(33) Macrae, C. F.; Sovago, I.; Cottrell, S. J.; Galek, P. T. A.; McCabe, P.; Pidcock, E.; Platings, M.; Shields, G. P.; Stevens, J. S.; Towler, M.; Wood, P. A. Mercury 4.0: from visualization to analysis, design and prediction. *J. Appl. Crystallogr.* **2020**, *53*, 226−235.
(34) Sheldrick, G. M. *SADABS-2008/1 - Bruker AXS Area Detector Scaling and Absorption Correction*; Bruker AXS: Madison, WI, 2008.
(35) Sheldrick, G. M. Crystal Structure Refinement with SHELXL. *Acta Crystallogr., Sect. C: Struct. Chem.* **2015**, *71*, 3−8.
(36) (a) Cordero, B.; Gómez, V.; Platero-Prats, A. E.; Revés, M.; Echeverría, J.; Cremades, E.; Barragán, F.; Alvarez, S. Covalent radii revisited. *Dalton Trans.* **2008**, 2832−2838. (b) Bondi, A. Van der Waals Volumes and Radii. *J. Phys. Chem.* **1964**, *68*, 441−451.
(37) Mingos, D. M. P.; May, A. S. In *Chemistry of Metal Cluster Complexes*; Shriver, D. S., Kaesz, H. D., Adams, R. D., Eds.; VCH, 1990.
(38) Ceriotti, A.; Longoni, G.; Manassero, M.; Perego, M.; Sansoni, M. Nickel Carbide Carbonyl Clusters. Synthesis and Structural Characterization of $[Ni_8(CO)_{16}C]^{2-}$ and $[Ni_9(CO)_{17}C]^{2-}$. *Inorg. Chem.* **1985**, *24*, 117−120.
(39) Heaton, B. T.; Strona, L.; Pergola, R. D.; Vidal, J. L.; Schoening, R. C. Multinuclear Variable-temperature Nuclear Magnetic Resonance Study of Rhodium Carbonyl Clusters containing Encapsulated Heteroatoms: Ligand and Metal Polyhedral Rearrangements. *J. Chem. Soc., Dalton Trans.* **1983**, 1941−1947.
(40) MacLaughlin, S. A.; Taylor, N. J.; Carty, A. J. $Ru_5(CO)_{16}(\mu\text{-}PPh_2)(\mu_3\text{-}P)$: A Low-Nuclearity Cluster with a Partially Encapsulated Phophide. *Inorg. Chem.* **1983**, *22*, 1409−1411.
(41) Van Gastel, F.; Taylor, N. J.; Carty, A. J. Encapsulated Phosphides: $Ru_8(CO)_{21}(\mu_6\text{-}P)(\mu_4\text{-}PPh)(\mu_2\text{-}PPh_2)$, a Molecule with a Six-Coordinate Phosphorus Atom in a Condensed Cluster. *Inorg. Chem.* **1989**, *28*, 384−388.
(42) Cesari, C.; Ciabatti, I.; Femoni, C.; Iapalucci, M. C.; Zacchini, S. Capping $[H_{8-n}Ni_{42}C_8(CO)_{44}]^{n-}$ (n = 6, 7, 8) Octa-carbide Carbonyl Nanoclusters with [Ni(CO)] and [CuCl] Fragments. *J. Cluster Sci.* **2017**, *28*, 1963−1979.
(43) Bernardi, A.; Ciabatti, I.; Femoni, C.; Iapalucci, M. C.; Longoni, G.; Zacchini, S. Ni-Cu tetracarbide carbonyls with vacant Ni(CO) fragments as borderline compounds between molecular and quasi-molecular clusters. *Dalton Trans.* **2013**, *42*, 407−421.
(44) Femoni, C.; Iapalucci, M. C.; Longoni, G.; Zacchini, S.; Fedi, S.; Fabrizi de Biani, F. Nickel poly-acetylide carbonyl clusters: structural features, bonding and electrochemical behaviour. *Dalton Trans.* **2012**, *41*, 4649−4663.
(45) Bernardi, A.; Ciabatti, I.; Femoni, C.; Iapalucci, M. C.; Longoni, G.; Zacchini, S. Molecular nickel poly-carbide carbonyl nanoclusters: The octa-carbide $[HNi_{42}C_8(CO)_{44}(CuCl)]^{7-}$ and the deca-carbide $[Ni_{45}C_{10}(CO)_{46}]^{6-}$. *J. Organomet. Chem.* **2016**, *812*, 229−239.
(46) Femoni, C.; Iapalucci, M. C.; Longoni, G.; Zacchini, S.; Ciabatti, I.; Della Valle, R. G.; Mazzani, M.; Riccò, M. The Chemistry of Ni-Sb Carbonyl Clusters − Synthesis and Characterization of the $[Ni_{19}Sb_4(CO)_{26}]^{4-}$ Tetraanion and the Viologen Salts of $[Ni_{13}Sb_2(CO)_{24}]^{n-}$ Carbonyl Clusters. *Eur. Eur. J. Inorg. Chem.* **2014**, *2014*, 4151−4158.
(47) Ciabatti, I.; Fabrizi de Biani, F.; Femoni, C.; Iapalucci, M. C.; Longoni, G.; Zacchini, S. Selective synthesis of the $[Ni_{36}Co_8C_8(CO)_{48}]^{6-}$ octa-carbide carbonyl cluster by thermal decomposition of the $[H_2Ni_{22}Co_6C_6(CO)_{36}]^{4-}$ hexa-carbide. *Dalton Trans.* **2013**, *42*, 9662−9670.
(48) Xu, W. W.; Zeng, X. C.; Gao, Y. The structural isomerism in gold nanoclusters. *Nanoscale* **2018**, *10*, 9476−9483.
(49) Tian, S.; Li, Y.-Z.; Li, M.-B.; Yuan, J.; Yang, J.; Wu, Z.; Jin, R. Structural Isomerism in Gold nanoparticles Revealed by X-Ray Crystallography. *Nat. Commun.* **2015**, *6*, 8667.

https://dx.doi.org/10.1021/acs.inorgchem.0c02572
Inorg. Chem. 2020, 59, 16016−16026

(50) Berti, B.; Bortoluzzi, M.; Cesari, C.; Femoni, C.; Iapalucci, M. C.; Mazzoni, R.; Vacca, F.; Zacchini, S. Polymerization Isomerism in $[\{MFe(CO)_4\}_n]^{n-}$ (M = Cu, Ag, Au; n = 3, 4) Molecular Clusters Supported by Metallophilic Interactions. *Inorg. Chem.* **2019**, *58*, 2911−2915.
(51) Fu, J.; Morshedi, M.; Moxey, G. J.; Barlow, A.; Cifuentes, M. P.; Humphrey, M. G. Dynamic Permutational Isomerism in a closo-Cluster. *Chem. - Eur. J.* **2016**, *22*, 5128−5132.
(52) Berti, B.; Ciabatti, I.; Femoni, C.; Iapalucci, M. C.; Zacchini, S. Cluster Core Isomerism Induced by Crystal Packing Effects in the $[HCo_{15}Pd_9C_3(CO)_{38}]^{2-}$ Molecular Nanocluster. *ACS Omega* **2018**, *3*, 13239−13250.
(53) (a) Bullock, L. M.; Field, J. S.; Haines, R. J.; Minshall, E.; Smit, D. N.; Sheldrick, G. M. Synthesis and structural characterization of $[Ru_8(\mu_8\text{-}P)(\mu_2\text{-}\eta^1,\eta^6\text{-}CH_2C_6H_5)(\mu_2\text{-}CO)_2(CO)_{17}]$: example of phosphorus encapsulated in a square anti-prism of ruthenium atoms and of an unusual coordination mode for the benzyl group. *J. Organomet. Chem.* **1986**, *310*, C47−C50. (b) Bullock, L. M.; Field, J. S.; Haines, R. J.; Minshall, E.; Moore, M. H.; Mulla, F.; Smit, D. N.; Steer, L. M. Condensation as well as trinuclear products from the reaction of triruthenium dodecacarbonyl with diphenylphosphine. *J. Organomet. Chem.* **1990**, *381*, 429−456.
(54) (a) Charalambous, E.; Heuer, L.; Johnson, B. F.G.; Lewis, J.; Li, W.-S.; McPartlin, M.; Massey, A. D. High nuclearity ruthenium cluster compounds containing phosphorus ligands; synthesis and crystal structure of $[Ru_6(CO)_{11}(P^tBu)_4]$, $[Ru_7(CO)_{14}(P^tBu)_4]$, and $[H_3Ru_9(CO)_{20}(\mu_7\text{-}P)(P^tBu_3)]$. *J. Organomet. Chem.* **1994**, *468*, C9−C12. (b) Frediani, P.; Bianchi, M.; Salvini, A.; Piacenti, F.; Ianelli, S.; Nardelli, M. Behaviour of $[Ru(CO)_2(MeCO_2)_2(PBu^n_3)_2]$ in the presence of carbon monoxide and/or hydrogen: crystal structure of $[Ru_6(\mu\text{-}H)(CO)_{10}(\mu\text{-}PHBu^n)(\mu\text{-}PBu^n_3)_2(\mu_6\text{-}P)]$. *J. Chem. Soc., Dalton Trans.* **1990**, 165−171.
(55) (a) Liu, S.-T.; Hu, S.; Chang, F.; Liu, Y.-C.; Ding, E.-R.; Wu, B.-F.; Zhao, Z.-R. Substituted boat-shaped Co_6 carbonyl cluster derivatives containing a semi-interstitial P atom and both bridging dithiolate and heterocyclic phosphido ligands. *Polyhedron* **2002**, *21*, 1073−1080. (b) Lang, H.; Huttner, G.; Zsolnai, L.; Mohr, G.; Sigwarth, B.; Weber, U.; Orama, O.; Jibril, I. Diphospor, phosphor-, arsen- und antimonate als clusterbaugruppen. *J. Organomet. Chem.* **1986**, *304*, 157−179.
(56) Scoles, L.; Sterenberg, B. T.; Udachin, K. A.; Carty, A. J. Transformation of μ_4-Phosphinidenes at an Ru_5 Center: Isolation and Structural Characterization of Hydroxyphospinidene Cluster Acids, Fluorophosphinidenes, and a Novel μ_5-Phosphide. *Inorg. Chem.* **2005**, *44*, 2766−2773.
(57) Femoni, C.; Iapalucci, M. C.; Ruggieri, S.; Zacchini, S. From Mononuclear Complexes to Molecular Nanoparticles: The Building up of Atomically Precise Heterometallic Rhodium Carbonyl Nanoclusters. *Acc. Chem. Res.* **2018**, *51*, 2748−2755.
(58) (a) Femoni, C.; Bussoli, G.; Ciabatti, I.; Ermini, M.; Hayatifar, M.; Iapalucci, M. C.; Ruggieri, S.; Zacchini, S. Interstitial Bismuth Atoms in Icosahedral Rhodium Cages: Syntheses, Characterizations, and Molecular Structures of the $[Bi@Rh_{12}(CO)_{27}]^{3-}$, $[(Bi@Rh_{12}(CO)_{26})_2Bi]^{5-}$, $[Bi@Rh_{14}(CO)_{27}Bi_2]^{3-}$, and $[Bi@Rh_{17}(CO)_{33}Bi_2]^{4-}$ Carbonyl Clusters. *Inorg. Chem.* **2017**, *56*, 6343−6351. (b) Femoni, C.; Funaioli, T.; Iapalucci, M. C.; Ruggieri, S.; Zacchini, S. Rh-Sb Nanoclusters: Synthesis, Structure, and Electrochemical Studies of the Atomically Precise $[Rh_{20}Sb_3(CO)_{36}]^{3-}$ and $[Rh_{21}Sb_2(CO)_{38}]^{5-}$ Carbonyl Compounds. *Inorg. Chem.* **2020**, *59*, 4300−4310.
(59) Zacchini, S. Using Metal Carbonyl Clusters To Develop a Molecular Approach towards Metal Nanoparticles. *Eur. J. Inorg. Chem.* **2011**, *2011*, 4125−4145.
(60) (a) Jin, R.; Zeng, C.; Zhou, M.; Chen, Y. Atomically Precise Colloid Metal Nanoclusters and Nanoparticles: Fundamentals and Opportunities. *Chem. Rev.* **2016**, *116*, 10346−10413. (b) Chakraborty, I.; Pradeep, T. Atomically Precise Clusters of Noble Metals: Emerging Link between Atoms and Nanoparticles. *Chem. Rev.* **2017**, *117*, 8208−8271.
(61) (a) Yao, Q.; Chen, T.; Yuan, X.; Xie, J. Toward Total Synthesis of Thiolate-Protected Metal Nanoclusters. *Acc. Chem. Res.* **2018**, *51*, 1338−1348. (b) Narouz, M. R.; Osten, K. M.; Unsworth, P. J.; Man, R. W. Y.; Salorinne, K.; Takano, S.; Tomihara, R.; Kaappa, S.; Malola, S.; Dinh, C.-T.; Padmos, J. D.; Ayoo, K.; Garrett, P. J.; Nambo, M.; Horton, J. H.; Sargent, E. H.; Häkkinen, H.; Tsukuda, T.; Crudden, C. M. N-heterocyclic carbene-functionalized magic-number gold nanoclusters. *Nat. Chem.* **2019**, *11*, 419−425.

https://dx.doi.org/10.1021/acs.inorgchem.0c02572
Inorg. Chem. 2020, 59, 16016−16026